PROFESORSKÁ PŘEDNÁŠKA

CRACK-RESISTANT BINDERS FOR DURABLE CONCRETE STRUCTURES

doc. Ing. VÍT ŠMILAUER, Ph.D., DSc.

ČVUT
ČESKÉ VYSOKÉ UČENÍ TECHNICKÉ V PRAZE

České vysoké učení technické v Praze
Fakulta stavební

Czech Technical University in Prague
Faculty of Civil Engineering

Crack-resistant binders for durable concrete structures

Trhlinkovzdorná pojiva pro trvanlivé betonové konstrukce

Doc. Ing. Vít Šmilauer, Ph.D., DSc.

Praha, 2022

Summary

Concrete durability and maintenance present dominant factors for the service life of concrete elements. Pressure on the construction speed in all sectors of civil engineering in the last decades has preferred cements with a high early strength gain. Such elements exposed to external environments often show degradation in the form of visible cracks, increased permeability, decreased durability and service life. An example is an unreinforced cement concrete pavement, where 75% of Czech pavements show visible cracks already after 15 years of service.

The reason for the low resistance of concretes and binders to the formation of visible cracks is mainly the rate of chemical shrinkage, which is reflected in the high early strength gain. Rapid volume shrinkage leads to the formation of microcracks. They are proved both experimentally by means of 3D X-ray tomography and numerically by a multiscale model for strength scaling. Temperature, humidity and freezing cycles lead to the microcracks coalescence into visible cracks with subsequent concrete disintegration.

This book quantifies the crack resistance of binders by a restrained ring shrinkage test. 23 cements were evaluated, having different Blaine fineness and substitution level by ground granulated blast furnace slag. The beneficial effect of slow-hardening binders has been unequivocally confirmed, either by lower fineness or by clinker replacement. From these tests, a crack-resistant binder was designed, corresponding to CEM II/B-S 42.5 N cement.

In cooperation with the Road and Motorway Directorate of the Czech Republic and the Skanska, a.s. contractor, the crack-resistant binder was used in the pilot construction of an almost 9 km long concrete pavement on the D1 highway Přerov-Lipník nad Bečvou. This is the first major use of road Portland slag cement in the Czech Republic with a concrete volume exceeding 54 000 m^3. A long-term monitoring system was set up on a $3.5 \times 5.0 \times 0.29$ m concrete slab using 18 vibrating wire gauges and other sensors. The results after 3 years show consistent behavior with numerical models and the pavement remains free of visible cracks. The ongoing revision of road cement codes is a proof that extending the service life is more important than saving a few days during construction.

Souhrn

Trvanlivost betonu a údržba představuje dominantní faktory pro životnost betonového prvku. Tlak na rychlost výstavby ve všech odvětvích stavebnictví v posledních desítkách let vedly k preferenci cementů s rychlými počátečními pevnostmi. Takové prvky vystavené externímu prostředí vykazují často degradaci ve formě viditelných trhlin, které zvyšují permeabilitu, snižují trvanlivost a životnost. Klasickým příkladem jsou nevyztužené cementobetonové kryty, kde 75% českých krytů vykazuje viditelné trhliny po 15 let provozu.

Přičinou malé odolnosti betonů a pojiv ke vzniku viditelných trhlin je zejména rychlost chemického smrštění, která se odráží v rychlosti počátečních pevností. Rychlá objemová deformace vede na vznik mikrotrhlin, které jsou prokázány jak experimentálně pomocí 3D rentgenové tomografie tak i numericky pomocí víceúrovňového modelu pro škálování pevnosti. Teplotní, vlhkostní a mrazové cykly vedou ke spojování mikrotrhlin do viditelných trhlin s následným rozpadem betonu.

Tato kniha kvantifikuje odolnost pojiv ke vzniku trhlin pomocí prstencových testů vázaného smrštění. Na nich bylo ověřeno 23 cementů s rozdílnou jemností mletí a substitucí mleté vysokopecní granulované strusky. Jednoznačně se potvrdil blahodárný účinek pomalých nárůstů pevností ať už pomocí nižší jemnosti mletí či nahrazením slínku. Z těchto zkoušek bylo navrženo trhlinkovzdorné pojivo, které odpovídá cementu CEM II/B-S 42,5 N.

Ve spolupráci s Ředitelstvím silnic a dálnic ČR a zhotovitelem Skanska, a.s. bylo trhlinkovzdorné pojivo použito při výstavbě téměř 9 km cementobetonového pilotního krytu na dálnici D1 Přerov-Lipník nad Bečvou. Jedná se o první větší použití silničního portlandského struskového cementu v Česku s objemem betonu přes 54 000 m^3. Na úseku je dlouhodobě monitorována jedna deska cementobetonového krytu rozměrů $3,5 \times 5,0 \times 0,29$ m pomocí 18 strunových tenzometrů a dalších čidel. Výsledky po 3 letech ukazují na konzistentní chování s numerickými modely a kryt zůstává prostý viditelných trhlin. Probíhající revize předpisů pro silniční cementy je důkazem toho, že prodloužení životnosti je důležitější než úspora několika dnů během výstavby.

Key words: crack-resistant binders, durability, service life, ring shrinkage test, calorimetry, concrete road pavement

Klíčová slova: trhlinkovzdorná pojiva, trvanlivost, životnost, smršťující prstence, kalorimetrie, cementobetonový kryt

Contents

1 Historical perspective **6**

2 Causes and impacts of cracking **7**

3 Hydration of Portland cement and consequences **10**
3.1 Microcrack evolution due to autogenous shrinkage 11
3.2 Effect of drying shrinkage 13
3.3 Stability of crack growth 13

4 Multiscale model for strength scaling **15**

5 Crack-resistant road cements **17**
5.1 Restrained ring test 19
5.2 Hygro-mechanical simulations 22
5.3 Pilot highway project 23
5.3.1 Long-term monitoring 25
5.3.2 Characteristic summer slab performance 31
5.3.3 Static load test 32

6 Conclusions and outlook **33**

7 References **33**

8 Author's main achievements **37**

9 Curriculum vitae **40**

1 Historical perspective

Concrete belongs to the most man-made material, currently annually exceeding the world consumption of 1 m^3 / capita on average. Enhancing the durability of concrete structures became accented for sustainable development in the 21^{st} century. Many examples in history prove that concrete can withstand a long service time, e.g. unreinforced lime-pozzolan cement of Pantheon in Rome, the first concrete pavement in Bellefontaine, Ohio, USA from 1891, a reinforced concrete bridge from the 1890s in Krásno nad Kysucou, Slovakia, a concrete highway pavement on A18 in Poland from 1938, light fortification bunkers in Czechoslovakia from the 1930s, the concrete Hoover dam from 1935, a bridge in Bechyně from 1938, the Orlík dam from 1961.

Systematic studies on durability carried out in the USA after the 1930s stated that concrete cracking is the most predominant factor, resulting from the use of high-early strength cements [19]. The need for fast construction schedules generally increased the C_3S contents and raised the Blaine fineness in cement while decreasing the water-to-cement ratio (w/c); such a transition led from crack-resistant cements to crack-prone concretes. The shift can be manifested in the strength evolution of Type I general purpose Portland cements in the US between the 1950s and 1994, see Fig. 1 [3]. The study of the Iowa highway deterioration led John Lemish to conclude in 1969 that "Concretes that gain strength slowly are related to good performance" [5].

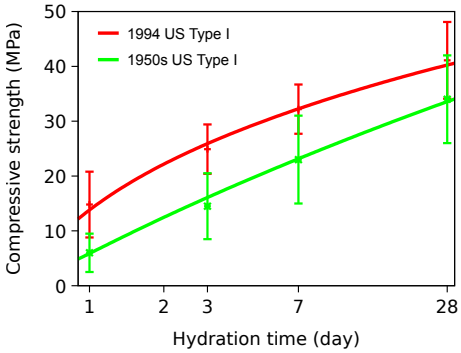

Figure 1: Compressive strength of cements produced in the 1950s (193 samples) and 1994 (>2150 samples) [3].

The advent of high performance concrete (28 day compressive strength exceeding 55 MPa) in the 1970s brought controversy to the topic of durability. The reduction of water contents led to smaller capillary porosity and lower permeability, in principle beneficial in slowing down several possible detrimental

transport phenomena. On the other hand, such concretes exhibit high elastic modulus, high brittleness, low creep and high autogenous shrinkage, leading generally to cracking. In this regard, durable concrete needs to minimize not only permeability on lab specimens but also cracking *in situ*.

The general need for construction speed practically eliminated low early strength cements from the market. Visible cracks became an essential part of structural concrete, generally impairing durability. The worst situation is obvious in concrete pavements, where slabs of unreinforced concrete are often exposed to drying/wetting cycles, temperature fluctuations, mechanical loads and freeze/thaw exposure with de-icing chemicals. Since concrete pavements belong to critical transport infrastructure, there is enough data from monitoring, maintenance and statistics for research.

Fig. 2 shows the deterioration of selected Czech concrete pavements as a function of the service time. They were cast mainly after 1990 and monitor 887 lane-km out of ∼1650 current lane-km [8]. 75% of such concrete pavements show visible cracking after 15 years, decreasing the service life to likely 25-30 years. Several sections were removed even after a few years due to surface cracking. This is in contrast with old concrete pavements, particularly the D1 highway built in the 1970s and 1980s, where concrete has lasted for over 40 years without significant cracking problems.

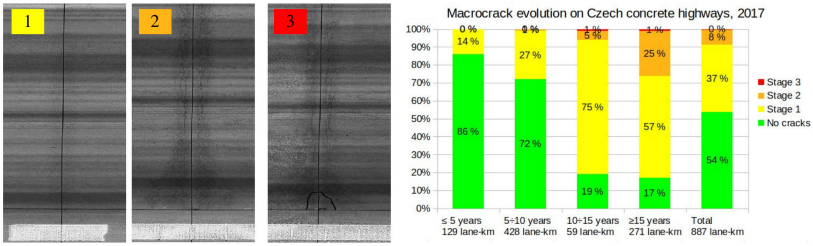

Figure 2: Deterioration of Czech concrete pavements built after 1990 [8].

Fig. 3 shows two examples of surface cracking; a plain concrete pavement on the D1 highway km 237.400 cast ∼2004 and a reinforced parapet wall built in 2008 on CTU campus. The wall indicates that steel reinforcement mitigates cracks only partially, crack-resistant binders would eliminate cracks completely.

2 Causes and impacts of cracking

Concrete is a quasi-brittle material with a low tensile strength thus susceptible to tensile cracking. Environmental loadings, mechanical loading and

Figure 3: Cracks in a concrete pavement after $\sim$17 years and in a parapet wall after 13 years.

deleterious reactions belong to the three common causes, which can be further sorted out into physical and chemical subcategories. The Transportation Research Board in the USA, a division of the National Research Council ad-

ministered also by the National Academy of Sciences, listed common crack types with regards to their origin and appearance [15]. Fig. 4 shows a modified version, supplemented with indicative times. It should be noted that the listed causes remain rather on the concrete scale, uncapturing lower material scales.

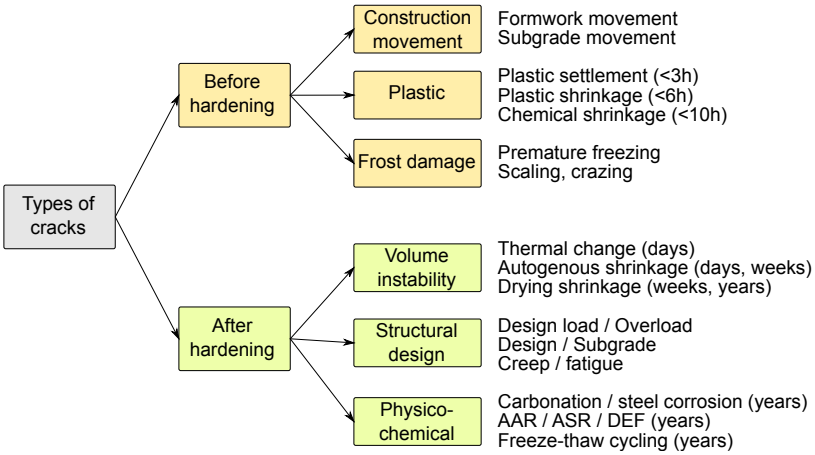

Figure 4: Common causes for concrete cracking with indicative times [15].

Cracking has generally a high impact on durability, opening concrete surface and increasing its permeability and ingress for water, ions or gases. For example, a crack width of 0.1 mm decreases the initiation time 2.6× for chloride-induced reinforcement corrosion with a 35 mm concrete cover [12].

Autogenous and drying shrinkage are practically inevitable in any concrete structure and generally lead to cracking on different scales. Autogeneous shrinkage is generally pronounced on $w/c \leq$0.42, affecting the whole concrete volume mostly up to 1 month. Drying shrinkage is the result of diffusion-driven moisture transport, affecting adversely the surface of concrete and causing rather shallow cracks in the $mm - cm$ range.

The mix design plays a crucial role in the propensity for concrete cracking. The most important parameter is the w/c ratio, where $w/c \leq$0.5 leads to the depercolation of capillary porosity thus efficiently reducing permeability. However, going to $w/c \leq$0.38 leads to high autogenous shrinkage, higher strength and modulus, higher brittleness and reduced creep [15]. Low cement contents and slow hardening cements were found beneficial for crack-resistant and durable concrete [5, 15].

3 Hydration of Portland cement and consequences

Portland cement, patented in 1824, binds efficiently mixing water into hydration products. The *degree of hydration* describes the average state of microstructure, which can be approximated conveniently by [25]

$$\mathrm{DoH}(t) = 1 - \frac{m_c(t)}{m_c(0)} \approx \frac{Q(t)}{Q(\infty)} \approx \frac{m_{nw}(t)}{m_{nw}(\infty)} \approx \frac{\varepsilon_{CS}(t)}{\varepsilon_{CS}(\infty)}, \tag{1}$$

where $m_c(t)$ is the cement mass, $Q(t)$ the released heat, $m_{nw}(t)$ the non-evaporable (chemically bound) water, and $\varepsilon_{CS}(t)$ the chemical shrinkage known as Le Chatelier's contraction. In Portland-based binders, chemical shrinkage attains values around 9%. The approximation by C_3S hydration corresponds to the water / C_3S mass ratio of 0.418 and yields

$$\begin{aligned} \mathrm{C_3S} + 5.3\mathrm{H} &\rightarrow \mathrm{C_{1.7}SH_4} + 1.3\mathrm{CH}, && (2)\\ 1 + 1.34 &\rightarrow 1.52 + 0.61, && (3)\\ 2.34 &\rightarrow 2.13, && (4)\\ 1 &\rightarrow 0.91, && (5) \end{aligned}$$

where the numbers capture volume fractions.

Autogenous shrinkage is defined as a volume change under sealed conditions, i.e. without any external moisture transfer. Chemical shrinkage practically equals to autogenous shrinkage up to around the final setting time, when a load-carrying solid skeleton distributes internal load. Fig. 5 shows such a characteristic behavior of the cement paste, with data combined from two resources [4, 16] and extended by the CEMHYD3D hydration model.

The difference between chemical and autogenous shrinkage remains within the microstructure, mostly in the form of empty capillary pores. Relative humidity at 90 days drops to 0.96 for $w/c = 0.50$ and 0.82 for $w/c = 0.20$ [13]. Disjoining pressure and capillary pressure are considered as two dominant mechanisms for relative humidity (RH) $\geq 50\%$. The Kelvin equation relates the radius of the largest water-filled capillary pore with relative humidity (values for standard conditions at 20°C) as

$$r = -\frac{2\gamma V_w}{RT \ln \frac{RH}{RH_S}} \approx \frac{-1.08 \cdot 10^{-9}}{\ln(RH) - \ln(0.97)} \ \ (\mathrm{m}). \tag{6}$$

The Laplace law in a cylindrical tube quantifies capillary tension in the water-filled pore

$$\sigma_{cap} = \frac{2\gamma}{r} \approx \frac{0.146}{r} \ \ (\mathrm{m, Pa}). \tag{7}$$

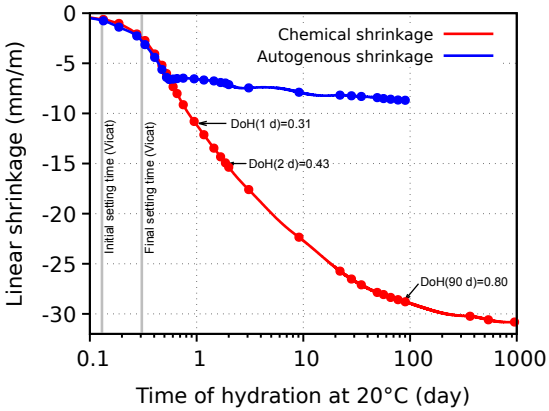

Figure 5: Characteristic chemical and autogenous shrinkage of a cement paste, CEM I 42.5 N - 52.5 N, $w/c = 0.40 - 0.45$.

Combined equations show that $RH = 0.90$ empties pores above $r = 14.4$ nm and induces σ_{cap} = 10.1 MPa in water. At lower relative humidity of $RH = 0.50$, pores under $r = 1.6$ nm remain full with σ_{cap} = 89.6 MPa.

3.1 Microcrack evolution due to autogenous shrinkage

The magnitude and rate of autogenous shrinkage has an impact on microcrack evolution. This can be demonstrated on a concrete mesostructure 50×50 mm, where 49% vol. is resolved as aggregates, 3% as an interfacial transition zone (ITZ) around the aggregates and 48% as a shrinking mortar. The simulation uses the MPS isotropic damage model with exponential softening for concrete creep and cracking within OOFEM software [23].

Fig. 6 imposes linear mortar deformation $-500 \cdot 10^{-6}$ within 2 or 4 days, corresponding to rates $-250 \cdot 10^{-6}$/day and $-125 \cdot 10^{-6}$/day. Creep characteristics are derived from the mortar, the tensile strength is assumed as 4 MPa at 28 days and the shrinkage is imposed at 0.5 day of hydration. The strength in ITZ is reduced to a half. The results show the opening of ITZ and microcrack formation up to 1 μm wide. Creep efficiently decreases elastic strain, which in turns leads to stress relaxation and less cracking. Although this numerical simulation is simplified in many ways, it illustrates the beneficial role of creep for microcrack formation.

Experimental evidence of microcracking during sealed hydration has been carried out recently at Imperial College London using nondestructive 3D X-ray microtomography [17, 18, 28]. Characteristic 3D images of microcracks are showed in Fig. 7 after 3.6 years of sealed hydration. The mean microcrack

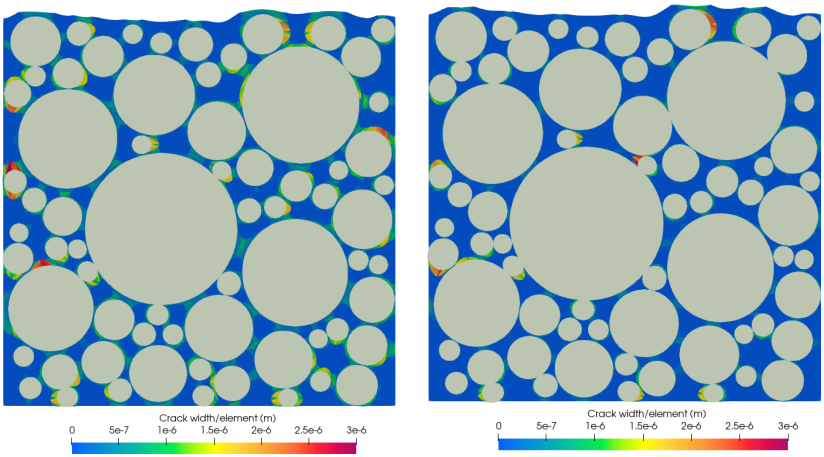

Figure 6: Crack evolution in concrete mesostructures 50×50 mm exposed gradually to shrinkage $-500 \cdot 10^{-6}$, shrinkage rates $-250 \cdot 10^{-6}$/day (left) and $-125 \cdot 10^{-6}$/day (right). Planar deformation enforced on vertical edges, deformations $1000\times$ exaggerated.

widths were found as 10-20 μm on 27 concretes; the density and connectivity increased with the decreasing water/binder (w/b) ratio and the increasing binder reactivity. Despite more microcracking at lower w/b ratios, oxygen permeability decreased, which shows that transport occurred primarily through the paste and not the microcracks. Those results are valid for samples cured at constant laboratory conditions, however, the microcracks tend to grow and interconnect due to exterior fluctuating environmental actions.

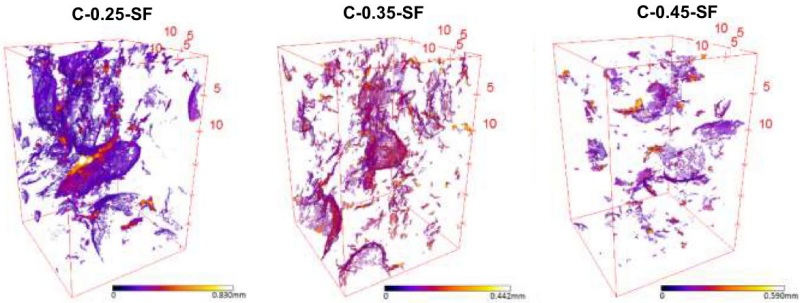

Figure 7: 3D X-ray microtomography of microcracks in $\approx 20 \times 20 \times 30$ mm box [28].

3.2 Effect of drying shrinkage

Drying shrinkage requires a moisture flow across a boundary. The rate of free shrinkage strain can be approximately related to the rate of relative humidity as

$$\dot{\varepsilon} = k_{sh}\dot{h}, \tag{8}$$

where k_{sh} is an empirical shrinkage ratio [1]. The crack growth can be visualized on a concrete mesostructure 50×50 mm using a weakly coupled hygro-mechanical model, see Fig. 8. The unit cell is exposed to 50% relative humidity from the top, with planar deformation enforced on vertical edges, and $k_{sh} = 3 \cdot 10^{-3}$ assigned to a shrinking mortar. Since the deformation localizes in a crack band with several finite elements, the crack width will reach easily over 10 μm. Drying causes cracking mainly up to approximately 20 mm from the top, while the decrease of the drying rate is effectively balanced by stress relaxation in the mesostructure.

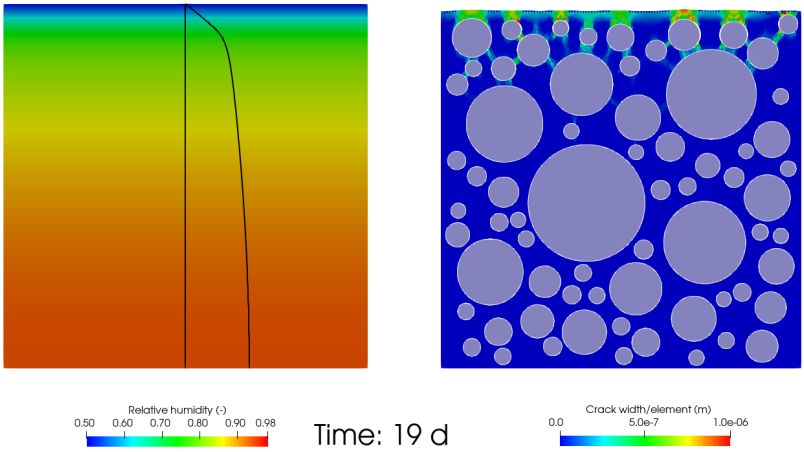

Figure 8: Field of relative humidity and crack evolution in a concrete mesostructure 50×50 mm due to top surface drying.

3.3 Stability of crack growth

Autogenous and drying shrinkage in the cement paste are restrained by aggregates, leading to high tensile stresses and microcracking. Figs. 6, 8 show such situations for both cases. The crack growth can be approximated in the form of parallel growing cracks and such a situation has been analysed in terms

of their stability and bifurcation. Let us consider two parallel cracks with initial lengths a_1, a_2 subjected to admissible variations $\delta a_1, \delta a_2$, see Fig. 9. Such a system is stable only if [2]

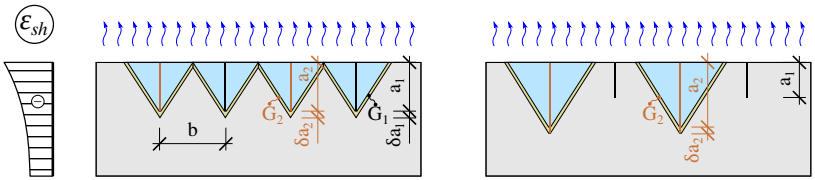

Figure 9: Growth of parallel cracks under a plane-stress problem.

$$2\delta^2 W = \sum_i \sum_j W_{ij}\delta a_i \delta a_j > 0, \tag{9}$$

$$W_{ij} = \frac{\partial^2 U}{\partial a_i \partial a_j} + \frac{\partial G_i}{\partial a_i}\delta_{ij} H(\delta a_i), \tag{10}$$

$$\delta a_i \geq 0 \text{ for } G_i = G_{f,i}, \tag{11}$$

$$\delta a_i = 0 \text{ for } 0 < G_i < G_{f,i}, \tag{12}$$

$$\delta a_i \leq 0 \text{ for } G_i = 0, \tag{13}$$

where W is the work of loads, U the strain energy of an elastic material, $G_i = -\partial U/\partial a_i$ the energy release rate of i^{th} growing crack. The critical state of equilibrium leads to bifurcation and to the growth of only single cracks a_2 while cracks a_1 become unloaded and they eventually close. The crack spacing b can be estimated from $\Delta U = G_f$, further assuming a half-space, a parabolic approximation of the shrinkage strain profile and a characteristic relative crack length as [2]

$$b \geq \frac{15 G_f}{E}\left(\frac{1-\nu}{\varepsilon_{sh}}\right)^2. \tag{14}$$

The realistic numbers for mature cement paste with $G_f = 30$ J/m^2, $E = 10$ GPa, $\nu = 0.25$, $\varepsilon_{sh} = 2 \cdot 10^{-3}$ results at $b \geq 6.3$ mm and crack width $w = 13$ μm. Taking into account mature concrete with $G_f = 100$ J/m^2, $E = 30$ GPa, $\nu = 0.25$, $\varepsilon_{sh} = 5 \cdot 10^{-4}$ leads to $b \geq 113$ mm and crack width $w = 57$ μm.

Crack growth analysis shows that durable concrete under environmental actions should primarily minimise microcracking and prevent its easy growth into visible cracks. This can be achieved by decreasing autogenous shrinkage ($w/c \geq 0.4$) and its rate using slow-hardening binders. This idea emerged

already in 1994 by P. K. Mehta [20], describing a transition from discontinuous microcracks to interconnected microcracks, accompanied with concrete spalling and disintegration.

4 Multiscale model for strength scaling

A multiscale model had been developed within Nanocem, a consortium of 23 large academic and 10 industrial partners mostly located in Europe. CTU in Prague became a founding member in 2004. It is worthy to mention a few academic partners that attended biannual meetings; Ecole Polytechnique Fédérale de Lausanne (EPFL), Aarhus University, Bauhaus-Universität Weimar, University of Aberdeen, Leeds University, Eidgenössische Materialprüfungs- und Forschungsanstalt (EMPA), Technical University of Denmark, Imperial College London, Technische Universität München, Technische Universität Wien, University of Sheffield. Notable industrial partners covered Aalborg Portland Group, Heidelberg Technology Center, LafargeHolcim, Titan Cement, or Sika Technology. An internal "Core project 10" allowed close cooperation with Technische Universität Wien and supported our Ph.D. student M. Hlobil.

The multiscale micromechanical model for the prediction of compressive strength of blended cement pastes is based on the hierarchical modeling of unit cells [11]. Elastic modulus, tensile strength and estimated fracture energy as homogenized fracture quantities are passed from a lower level higher. The extended and corrected version is depicted in Fig. 10 [27]. The model builds on assumption that a C-S-H globule is considered to be the only strain-softening component in the multiscale model, leading essentially to failure at each level. Softening occurs under excessive tension or compression using an elasto-damage constitutive law [11]. Fig. 10 shows the strength scaling for a mature cement paste of $w/c = 0.50$ and the length estimation of the fracture process zone as $R_c \approx 4EG_f/f_t^2$.

The hypothesis of the C-S-H globule failure (upscaled to the C-S-H failure) has been successfully tested on a ternary binder made from coal-combustion products, producing ettringite and C-S-H as the main hydration phases. The multiscale model yielded excellent strength prediction since C-S-H still presents the dominant percolating phase in the system [10].

The model allowed the prediction of compressive strength of blended cement pastes; a newly assembled database yielded 76 strength values for ordinary Portland cements, 5 for slag-blended cements, 5 for limestone-blended pastes, and 4 for finely ground quartz-blended pastes, see Fig. 11. A gradient of C-S-H was found, revealing a non-uniform distribution in the microstructure, captured by the parameter $\beta = 0.6$. It has to be emphasized that only the C-S-H globule failure was responsible for strength, the other phases behaved elastically.

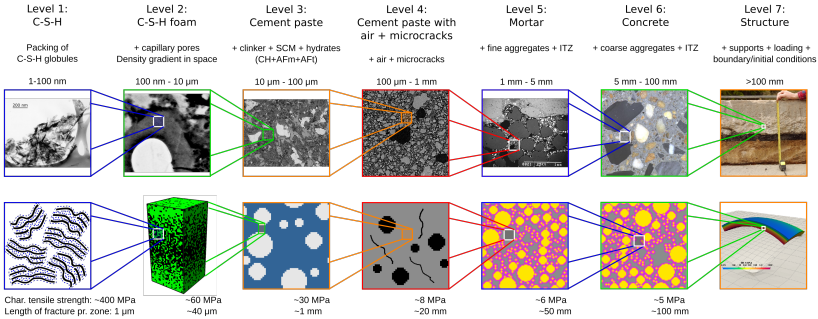

Figure 10: Multiscale model for strength scaling, extended from [11].

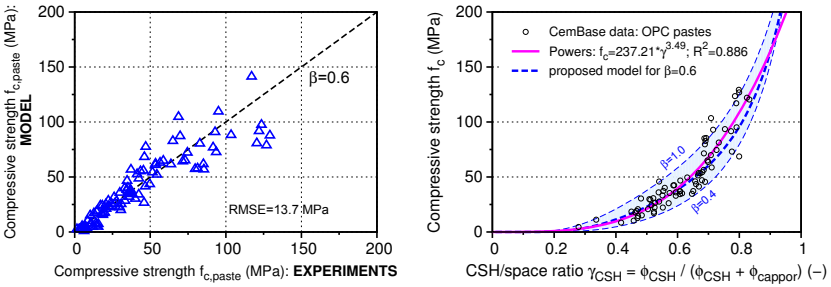

Figure 11: Validation of model-predicted compressive strength with experiments for $\beta = 0.6$ (left) and the C-S-H/space descriptor (right) [11].

The original version of the model predicted the tensile strength of the C-S-H globule as 320 MPa. However, direct measurements on ≈20 μm long cantilever beams from mainly the C-S-H phase revealed later that the theoretical globule's tensile strength must be much higher [21]. The tensile strength of 2500 MPa is much closer to a) theoretical strength as $f_t \approx E/10 = 57.1/10 = 5.71$ GPa, b) the results of a strongly cohesive polydisperse molecular model [7] and c) consistent with the N-A-S-H gel packing [22]. Fig. 12 shows the strength scaling and microstructure images for C-S-H$_{LD}$ and C-S-H$_{HD}$.

The model improvement occurred through introducing microcracks into Level 4, otherwise the strength scaling becomes mismatched between Level 2 and Level 4 by a factor between 3 and 8. The critical microcrack length was identified between 0.1 - 1.0 mm, reducing strength in a microcracked cement paste [27].

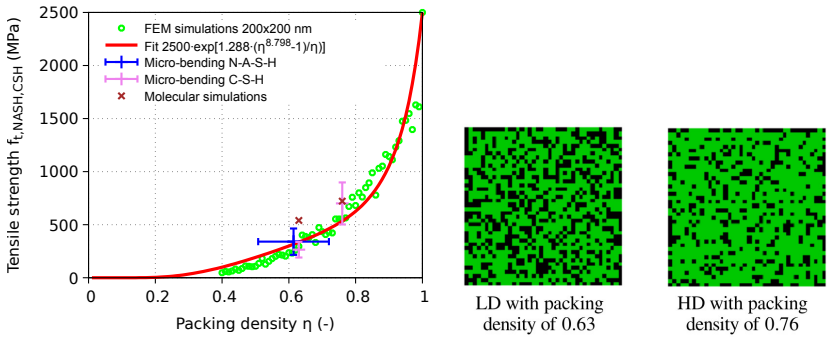

Figure 12: Strength scaling due to packing density of globules [27].

5 Crack-resistant road cements

The cracking of concrete structures was demonstrated on recent Czech concrete highways in Fig. 2. Crack-resistant binders have been debated for decades in the literature [5, 8, 9, 15, 19, 28]. The general conclusion on the paste (or binder) scale is to use slow-hardening binders or low alkali cements, both decreasing microcracking due to a lower rate of chemical shrinkage [5, 28]. There are at least four common methods how to achieve that objective:

- Changing clinker chemistry from alite-rich to belite-rich cements.
- Decreasing alkali content.
- Decreasing Blaine fineness.
- Substituting part of Portland clinker for less reactive supplementary cementititous materials.

The two last options are generally feasible from an industrial perspective, with small changes in cement production.

The differences in the hydration kinetics and the impact on cracking resistance will be exemplified on four road cements. Tab. 1 provides the current clinker composition from the Mokrá cement plant, the Czech Republic, where the Taylor mineral calculation yields C_3S 63.2%, C_2S 11.7%, C_3A 6.9%, and C_4AF 10.3%. The potential hydration heat corresponds to $Q_{pot} = 512$ J/g.

Table 1: Composition of Mokrá's Portland cement CEM I 42.5 R(sc) from May 31, 2018.

CaO	SiO_2	Al_2O_3	Fe_2O_3	SO_3	Na_2O	K_2O	MgO
63.8	20.7	4.8	3.4	3.2	0.16	0.75	1.4

Two Portland cements were ground from the same clinker, yielding a fine-

ness of 306 m^2/kg and 256 m^2/kg. The third blended binder was mixed using ground granulated blast furnace slag SMŠ 400. The fourth binder is from the 1970s when it was used for long-lasting concrete pavements in Czechoslovakia. The four cements are summarized as:

1. CEM I 42.5 R(sc) Mokrá with the Blaine fineness of 306 m^2/kg as a representative from the 2016-2018 commercial production range for concrete pavements.
2. CEM I 42.5 N Mokrá with the Blaine fineness of 256 m^2/kg.
3. A blended binder 75% CEM I 42.5 R(sc) + 25% SMŠ 400, which was intermixed in a concrete plant. The Blaine fineness yields 330 m^2/kg. This cement was used for $\sim$ 9 km of the D1 pilot highway section Přerov-Lipník nad Bečvou [9].
4. CEM I 32.5 R Maloměřice (formely SC70) used for Czech highway concrete pavements between the 1970s-1996. The concrete made from this cement served well for decades, for example over 40 years on the D1 highway between Mirošovice and Kývalka.

Binder's reactivity was determined by isothermal calorimetry, see Fig. 13. The hydration heat was measured in the TamAir calorimeter according to the prEN 196-11 method A changed for w/b=0.45. The heat evolution for CEM I 32.5 R Maloměřice remained unknown; it was matched by the compressive strength evolution with a similar Portland cement, ground to the Blaine fineness of 250 m^2/kg. The results show that reactivity is slowed down by the fineness, the clinker-slag replacement and the older wet technology production with unselective milling process.

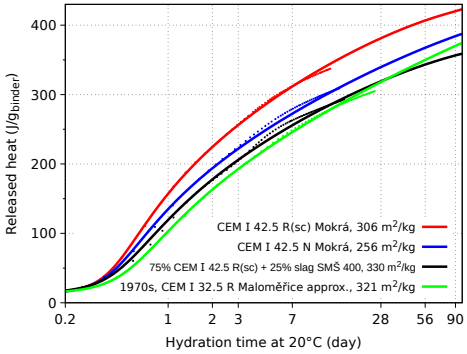

Figure 13: Released heat by isothermal calorimetry with approximations.

Fig. 14 summarizes the compressive and flexural strength evolution on standard mortars. Since a relationship between the degree of hydration and strength exists, the results from Mokrá's cements were fit on the curves from

Fig. 13 as

$$f_c = a\left(\frac{DoH - DoH_a}{1 - DoH_a}\right), \tag{15}$$

$$f_t = b\left(\frac{DoH - DoH_b}{1 - DoH_b}\right)^{0.65}, \tag{16}$$

with parameters a, DoH_a, b, DoH_b. The additional contribution of slag for compressive strength is treated by an additional function added after 7 days of hydration. The evolution of both strengths is high enough in all four binders for building concrete pavements.

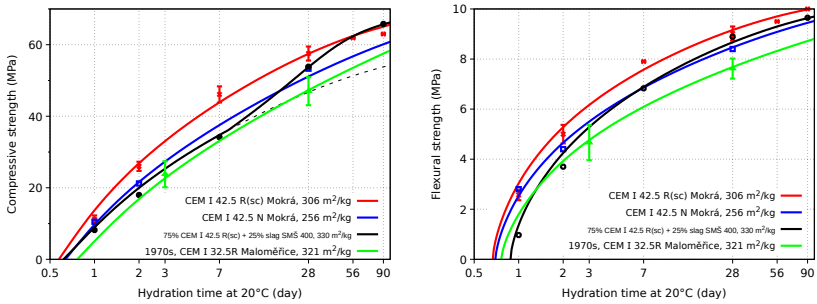

Figure 14: Compressive and flexural strength from four standard mortars.

5.1 Restrained ring test

The restrained ring test is a well-established method for testing the crack resistance of binders, mortars or concretes. The test was documented historically on at least 13 different ring dimensions and became adopted in several standards such as ASTM C1581 or AASHTO T334 [26]. The test is driven by tensile stresses induced by restrained autogenous and drying shrinkage. Stress relaxation and the tensile strength increase act beneficially for crack mitigation.

The first documented ring test was conducted by R. Carlson already in 1939–1942, followed by many researchers [5]. The ring test combines autogenous and drying shrinkage, creep, tensile strength evolution, fracture energy evolution and crack propagation. Several concrete structures, such as slabs or pavements, may exhibit cracking due to the combination of the aforementioned phenomena.

The short-time restrained ring test provided a strong correlation with long-term concrete cracking [5]; such an experiment was conducted on 28 various cements used for 104 panels $2.74 \times 1.22 \times 0.41$ m in size, placed around

the Green Mountain Dam, Colorado in 1943. The cracking time of the ring correlated well with the concrete surface cracking after 53 years; the sooner the ring cracked, the more severe cracking appeared later. Low alkali cements, coarser cements and lower C_3A cement performed the best.

Our ring test originates from R. W. Carlson's design but has a thinner steel ring to improve the deformation measurement [6], see Fig. 15. Mortars from the tested 4 cements and also other 19 cements were prepared mainly at $w/b = 0.45$ with the sand/binder ratio of 3:1. Drying at a relative humidity of 50% started after 24 hours of sealed curing. Four strain gauges measured the contraction of the steel ring, each binder was tested in at least two rings and the cracking time was averaged.

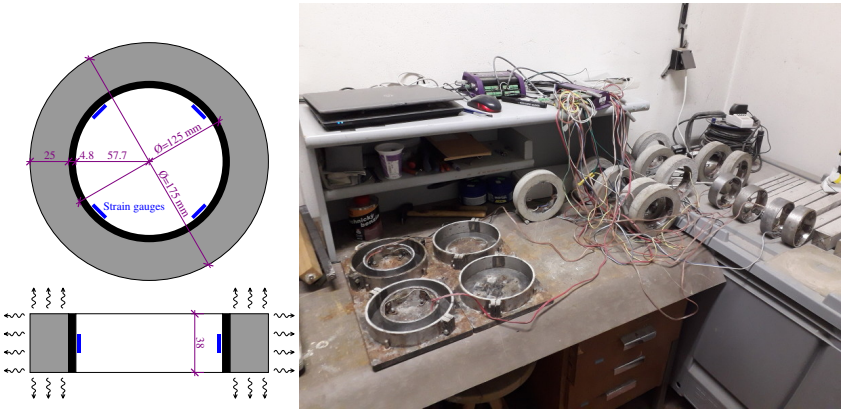

Figure 15: Ring geometry and the experimental setup.

Fig. 16 shows a characteristic strain evolution from three selected binders with a remarkable drop and macrocrack formation in the CEM I 42.5 R(sc) cement at 30 days. Strain fluctuations reflect a partly-stabilised RH environment in the range of 45-55%.

The results from 23 tested cements are summarized in Fig. 17. The description around a data point expresses the Blaine fineness and an average cracking time from at least two rings; the symbol $\geq$ means that the experiment was ceased without a crack. Fig. 17 justifies two factors acting beneficially for crack-resistant binders: low Blaine fineness and clinker substitution by less reactive slag. A violet line is a hypothetical threshold for binders that can survive at least 40 days without a crack in the ring test.

CEM I, CEM II/A-S and CEM II/B-S can belong to crack-resistant binders if the fineness stays reasonably low. Blue circles show Austrian norms and cements used for Austrian highway concrete pavements, generally with excellent durability. In Fig. 17, there are only two green-colored cements available on

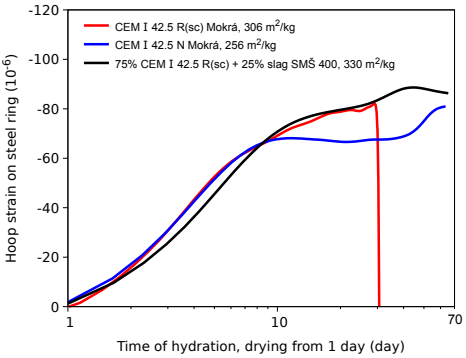

Figure 16: Hoop strain on the steel ring during the restrained shrinkage test.

the market, the other green-colored cements disappeared due to requirements for fast construction schedules.

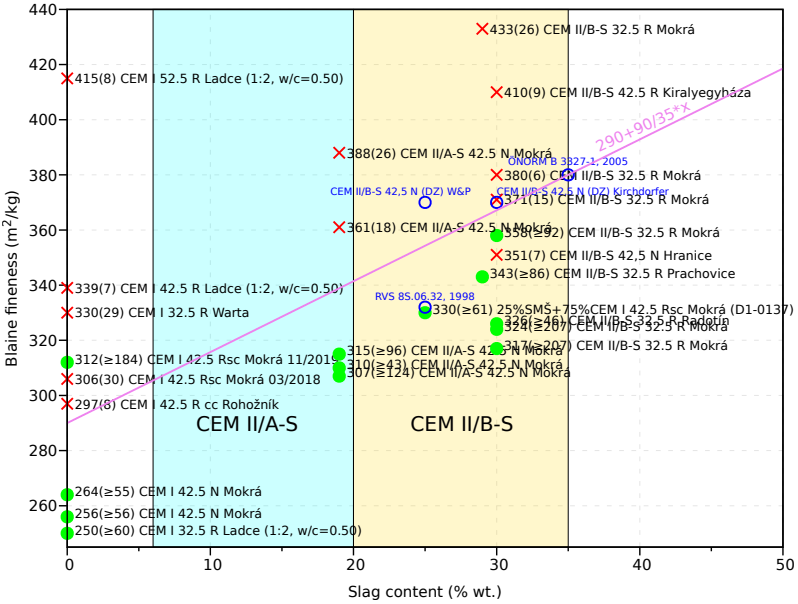

Figure 17: Results from 23 cements measured in the ring test.

5.2 Hygro-mechanical simulations

A hygro-mechanical model is able to capture the ring behavior, as demonstrated in the COST TU1404 benchmark [26]. The relative humidity field, h, stems from the water mass balance equation

$$\frac{\partial w}{\partial h}\frac{\partial h}{\partial t} = \nabla \cdot [c(h)\nabla h]\,, \tag{17}$$

with the Bažant-Najjar moisture permeability function calibrated as

$$c(h) = 2.56 \cdot 10^{-3}\left(0.1 + \frac{1-0.1}{1+\left(\frac{1-h}{1-0.7}\right)^{10}}\right) \text{kg/m/day}. \tag{18}$$

The numbers capture mortar's behavior from the CEM I 42.5 R(sc) Mokrá cement with the Blaine fineness of 306 m^2/kg. For simplicity, the desorption isotherm used a constant slope $\frac{\partial w}{\partial h} = 196$ kg/m^3, the initial condition assumed a relative humidity of 0.98 and the surface flux uses a hygric exchange coefficient of $h_w = 0.28$ kg/m^2/day.

The solution of the mechanical problem uses a staggered approach with a known relative humidity field at a particular time step. A fixed crack model is combined with a viscoelastic model to obtain stress evolution and fracturing strain as

$$\sigma_{i+1} = \sigma_i + \bar{D}_{ve}\left(\Delta\varepsilon - \Delta\varepsilon'' - \Delta\varepsilon_{sh} - \Delta\varepsilon_T - \Delta\varepsilon_{cr}\right). \tag{19}$$

The viscoelastic model is based on B3/B4 solidification models, extended further for the effect of humidity evolution [14]. Fig. 18 shows schematically the Kelvin unit chain where the relative humidity controls viscosity and the flow term ε_f. In addition, the decrease of relative humidity slows down the equivalent time, which captures the creep reduction of dry concrete.

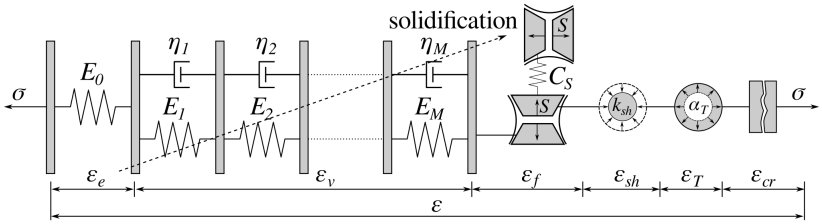

Figure 18: B3 creep model as a solidifying Kelvin chain [1]. Serial coupling with the cracking strain.

The rate of drying shrinkage strain is related to the rate of relative humidity as

$$\dot{\varepsilon}_{sh} = k_{sh}\dot{h} = 1.42 \cdot 10^{-3}\dot{h}, \tag{20}$$

while autogenous shrinkage is neglected. The uniaxial tensile strength at 28 days is estimated as 4.0 MPa, fracture energy at 28 days estimated as 50 J/m^2. The B3 model with equivalent times predicts ageing viscoelastic behavior with standard values from the mix design.

The finite element analysis of a restrained ring approximates geometry with a quarter of the top-half symmetric part. Both hygro-mechanical tasks use the same mesh. Interface elements are placed between steel and mortar rings, allowing the interface opening and a more compliant shear slip. In order to increase the strain localisation, an artificial notch was created by reducing the one cross-section area by 5%.

Fig. 19 shows the relative humidity field, the first principal stress at 30 days, just prior to the macrocrack formation over the whole mortar ring. The ring cracks at 31 days. Fig. 20 validates brittle failure at 31 days while the simulation retains a small strain value due to a nonzero shear stress between the steel and the mortar. Drying shrinkage is the major driving strain which is counterbalanced by stress relaxation and a tensile strength gain.

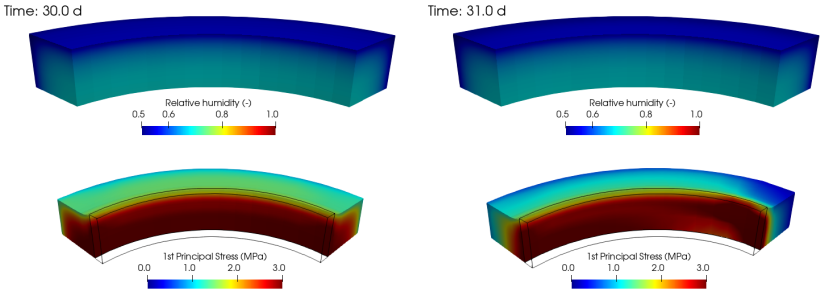

Figure 19: Hygro-mechanical simulation of $1/8$ of the ring test. Before cracking (left) and after cracking (right).

5.3 Pilot highway project

A pilot highway project started in 2017 as a joint activity among the Road and Motorway Directorate (ŘSD ČR), a contractor Skanska, a.s. and the Czech Technical University in Prague [24]. The objective was to test a durable concrete pavement with particular goals:

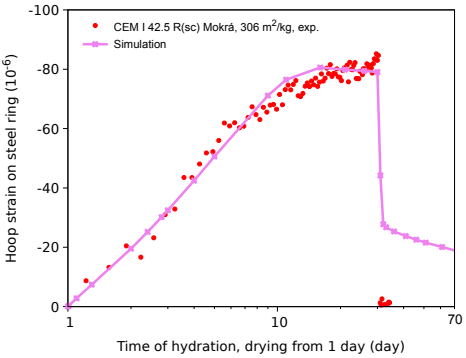

Figure 20: Validation of the ring test.

- Find a new concrete mix design for increased durability, even beyond current technical specifications.
- Test the new concrete on a pilot highway project.
- Short-term and long-term monitoring of selected pavement slabs and concrete pavement section.
- Thermo-mechanical numerical analyses with recommendations.
- Changing technical specifications up to our best knowledge.

The pilot highway project took place in the D1 section Přerov-Lipník nad Bečvou, the Czech Republic. 2 713 m was cast from the reference Portland cement CEM I 42.5 R(sc), Mokrá and 8 978 m made from a slag-blended, slow hardening binder 75% CEM I 42.5 R(sc) + 25% SMŠ 400, corresponding to CEM II/B-S 42.5 N. The characteristics of both binders were introduced previously in Section 5. The concrete pavement was cast during 06/2018-09/2019 with the summary in Tab. 2. The first concrete batch with the slag-blended binder was laid on July 23, 2018. The highway section was open to public on Dec 12, 2019.

Table 2: Length, area and volume on the pilot highway section.

Concrete with binder	Length (m)	Area (m^2)	Concrete volume (m^3)		
			Bottom	Top	Total
CEM I 42.5 R(sc), reference	2 713	57 205	14 962	3 399	18 361
CEM II/B-S 42.5 N = 75% CEM I 42.5 R(sc) + 25% SMŠ 400	8 978	176 340	43 982	10 754	54 736

The concrete from both binders had to fulfill the strength grade C30/37 at

28 days, such a requirement was achieved for both concretes, see Fig. 21. It is proved that the slag-blended binder provides a long-term strength evolution even within the monitored 59 days and extending to years. A small tensile strength drop of the reference binder shows likely the effect of microcracks.

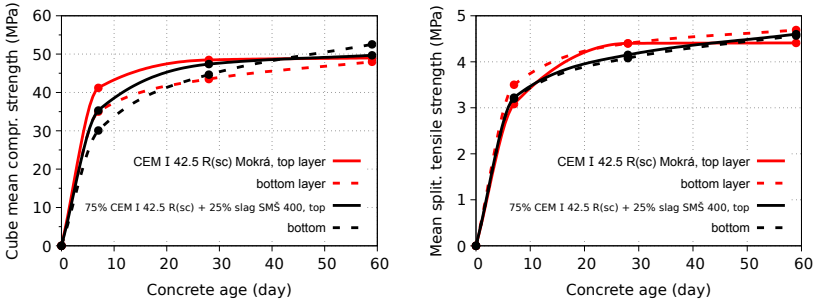

Figure 21: Compressive and tensile strength evolution of top and bottom concretes.

The de-icing salt-frost scaling test was carried out according to the ČSN 73 1326 method A with 100 cycles. Tab. 3 summarizes the results from the top layer, staying much below the limit of 1000 g/m^2. The slag-blended cement performed better *in situ* while the lab results show the opposite. Similar reversed trends were documented on dried specimens [5, Fig. 36].

Table 3: De-icing salt-frost scaling test, concrete age of 28 days.

Concrete with binder	Cube from lab (g/m^2)	Cylinder from pavement (g/m^2)
CEM I 42.5 R(sc), ref.	210±130	232±125
CEM II/B-S 42.5 N = 75% CEM I 42.5 R(sc) + 25% SMŠ 400	360±190	156±84

5.3.1 Long-term monitoring

A long-term monitoring system was designed and installed in one concrete pavement slab with dimensions of $3.5 \times 5.0 \times 0.29$ m. The system records temperature and strains at six measuring locations in a single slab, see Fig. 22. Each location contains three vibrating wire strain gauges located 50 mm from the surfaces and in the mid-height. All the gauges had integrated temperature sensors. In addition, one thermal gauge was placed 150 mm under the pave-

ment in order to deliver the sub-base temperature. Ambient air temperature and solar radiation sensors were installed as well.

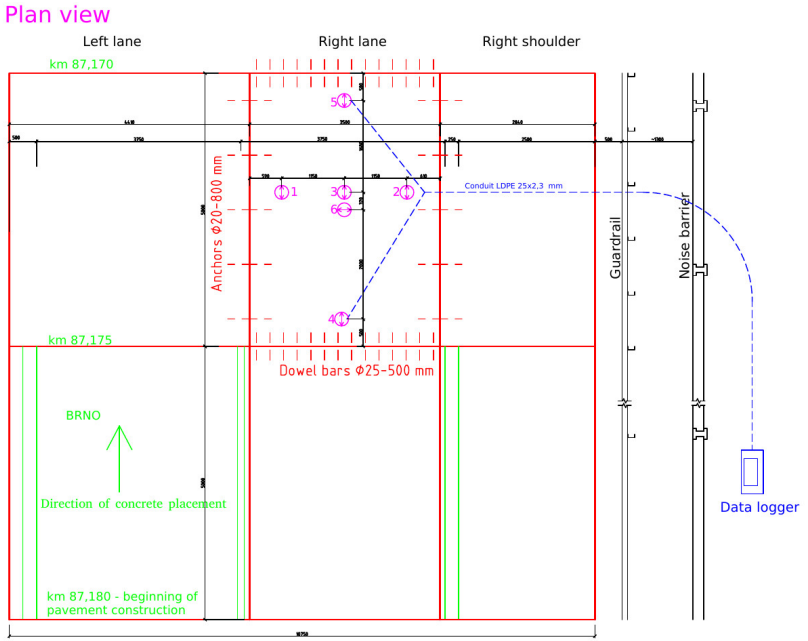

Figure 22: Plan view of the monitored concrete slab.

A two-step installation process ensured proper installation in a two-layer concrete placement. Protective covers hid the strain gauges before the placement, see Fig. 23. After the first finisher had passed, the covers were removed, the gauges put in their positions and the empty space filled back with concrete using hand vibrators, see Fig. 23. Finally, the top layer finalized the slab.

The monitored data are unique within the Czech Republic and scarce even worldwide. Fig. 24 shows the temperature evolution during 37 months on selected gauges. The maximum temperature reached 52.1°C after casting, other maximum temperatures yielded 46.0°C during summer and the minimum air temperature attained -15°C. Since the gauges have an offset of 50 mm from both surfaces, the linear temperature extrapolation to top surface gives extreme values of -9.0°C and 49.6°C.

Fig. 25 summarizes the temperature gradient, calculated from the temperature difference and assuming a linear temperature distribution. It is clear that solar radiation causes an additional increase of the surface temperature, leading to two-times higher negative gradients than the positive ones during the night cooling.

Figure 23: Vibrating wire gauges under protective covers. Detail at one assembled location.

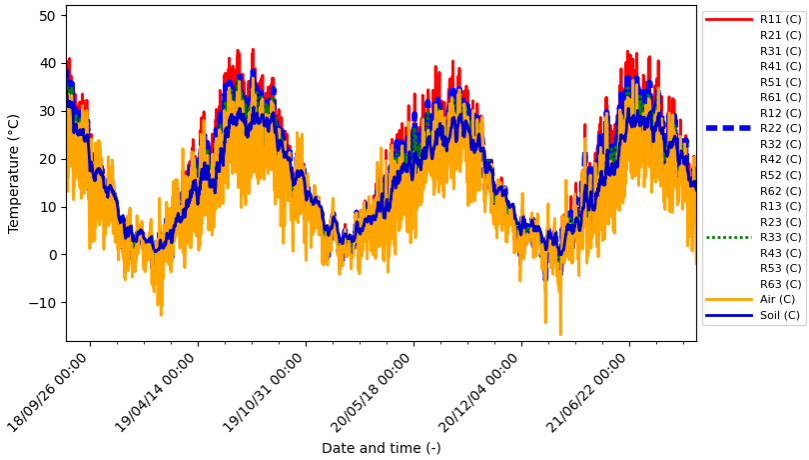

Figure 24: Temperature evolution at selected gauges, including the air and sub-base temperature.

A 2D heat transport model validated the first three days. The model takes into account a calibrated heat release from cement isothermal calorimetry.

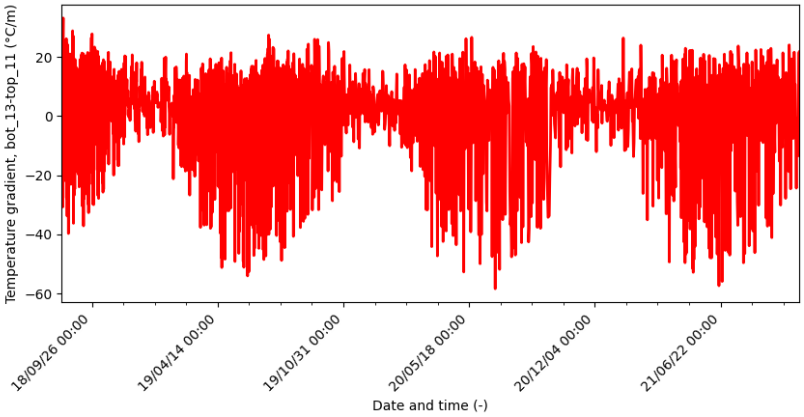

Figure 25: Temperature gradient over the thickness.

Boundary conditions include real-time data of solar irradiance, radiation and convective terms, the initial conditions were set according to measured temperatures, see Fig. 26.

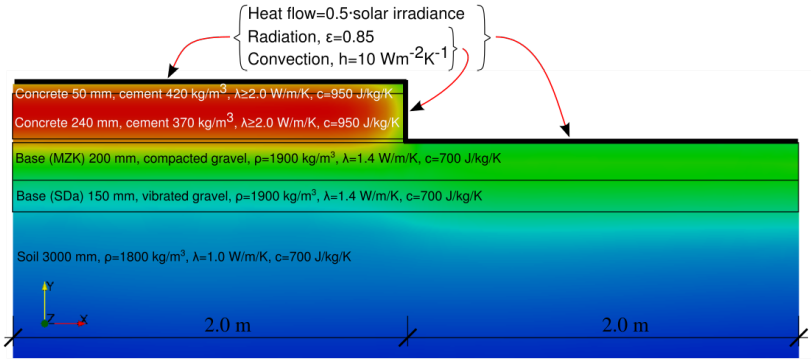

Figure 26: Geometry and boundary conditions for heat transport.

A strong formulation of heat transport is derived from energy balance as

$$-\nabla^T \mathbf{q}(\mathbf{x}) + \overline{Q}(\mathbf{x},t) = \rho(\mathbf{x}) c_V(\mathbf{x}) \frac{\partial T(\mathbf{x},t)}{\partial t}, \tag{21}$$

where $\mathbf{q}(\mathbf{x})$ (W/m^2) is the heat flux originating from conduction and various boundary conditions, $\overline{Q}(\mathbf{x},t)$ (W/m^3) represents the known heat source, $\rho(\mathbf{x})$ (kg/m^3) stands for the material density, $c_V(\mathbf{x})$ (Jkg^{-1}°C^{-1}) is the specific heat

capacity and $T(\mathbf{x}, t)$ (°C) represents the unknown temperature field.

Fig. 27 shows the validation, including the heat of hydration. It transpires that hydration contributes to approximately a 7°C increase. After two days, the hydration heat contributes negligibly.

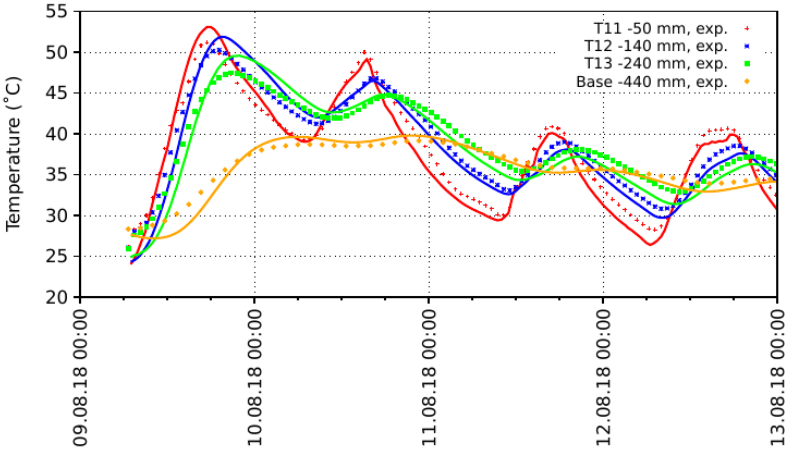

Figure 27: Three day validation after casting including hydration heat.

Vibrating strain gauges measure relative head displacements, which can be decomposed to

$$\varepsilon = \varepsilon_{ve} + \varepsilon_T + \varepsilon_{as} + \varepsilon_{ds} + \varepsilon_f + \dots, \tag{22}$$

where partial strains represent viscoelasticity, temperature effects, autogenous shrinkage, drying shrinkage, fracturing strain, etc.

Fig. 28 shows partial strains on the mid-plane, zeroed at 2 hours after the end of setting for all gauges. Autogenous shrinkage plays a dominant role in the first week, reaching -70 $\mu\varepsilon$ in the transversal direction. In the longitudinal direction, continuous casting led to prestressing, which adds additional strain. A small average drying shrinkage strain -30÷-120 $\mu\varepsilon$ is apparent after 3 years of drying.

The kinetics of slab drying can be estimated from small lab samples 60×100 mm exposed to 50% RH from the widest side. The calibration of the B4 model led to different asymptotic values $\varepsilon_{cem} = 800 \cdot 10^{-6}$, $\varepsilon_{au,cem} = 80 \cdot 10^{-6}$. Fig. 29 shows the lab sample and the average shrinkage for slab's edge gauge W52 when drying to 80% RH from the top.

The strain from gauge W52 was shifted by 40 $\mu\varepsilon$ to eliminate longitudinal prestressing. The predictions show that the slab will be drying for approxi-

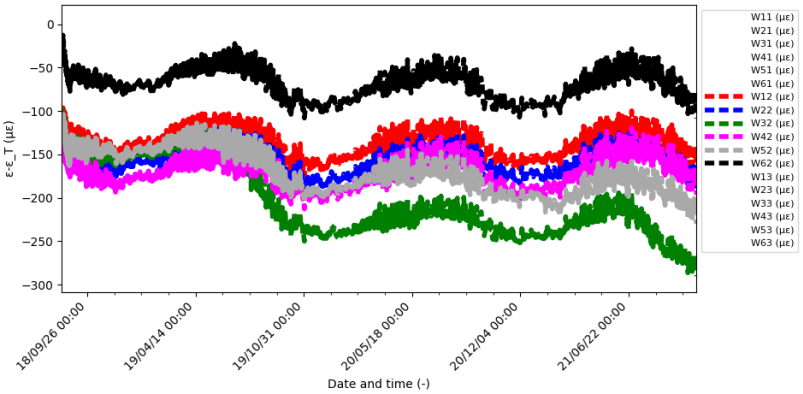

Figure 28: Partial strains on 18 gauges.

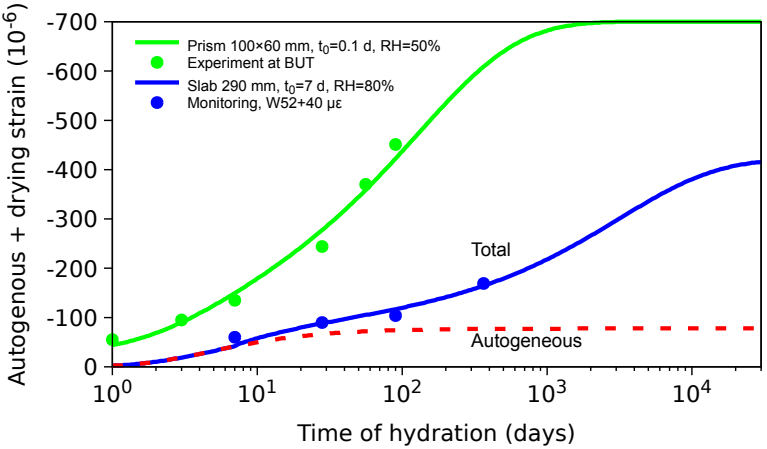

Figure 29: Shrinkage of the mid-plane.

mately 30 years. It should be mentioned that other gauges show smaller mid-plane shrinkage values, attributed likely to other partial strains and restraints.

The measured strains allowed calculating the curvature of the slab, assuming a planar deformation of the cross-section. Fig. 30 shows the total curvatures, capturing the temperature variations and demonstrating a slow positive drift due to top drying. The slab displacement can be obtained from double curvature integration, for example $\max\{\kappa_1, \kappa_2, \kappa_3\} = 0.5$ km^{-1} leads to the edge uplift $w = 0.5 \cdot 2.5^2/2 = 1.56$ mm.

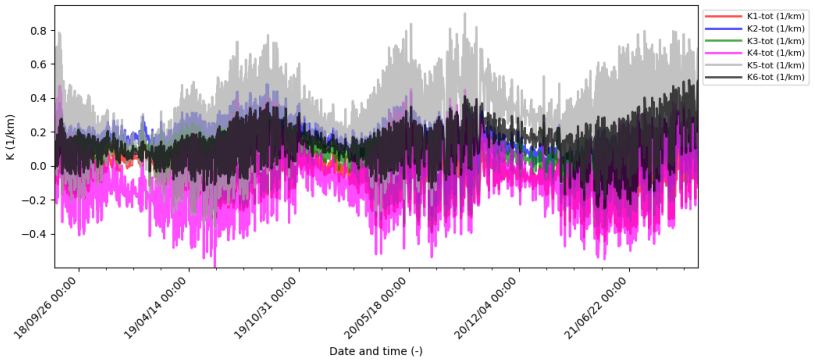

Figure 30: Total curvatures at six locations.

5.3.2 Characteristic summer slab performance

The measured data allow reconstructing a characteristic summer day with solar irradiance and air temperature changes. Fig. 31 validates temperatures at three gauges with reasonable agreement.

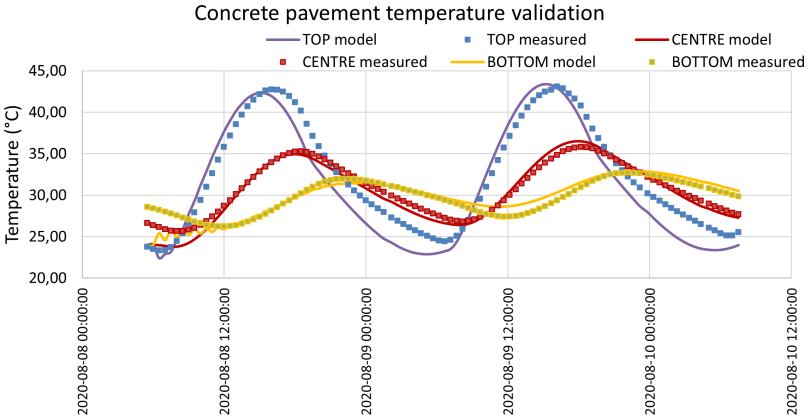

Figure 31: Validation of summer days.

The mechanical task uses a concrete slab resting on the Winkler-Pasternak foundation. The interface contact elements guarantee slab separation. Fig. 32 estimates the normal stress σ_{yy} when using the simplest elastic material with Young's modulus of 35 GPa. The maximum stress of 1.74 MPa occurs at 3 AM during the cooling phase, reaching about 40% of concrete's strength.

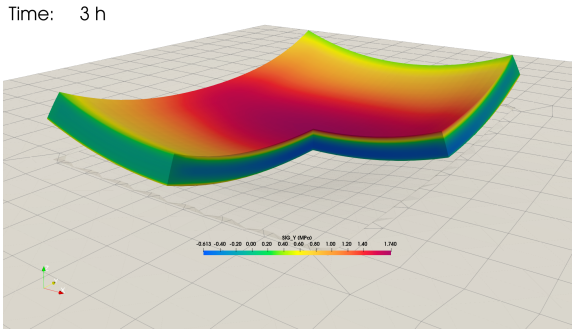

Figure 32: Normal stress σ_{yy} at 3 AM during a summer day.

5.3.3 Static load test

The static load test took place on the monitored slab on Apr 29, 2019. Two trucks were positioned to induce concave deformed shape, the axle loads on the slab had 109.6 and 116.6 kN. Fig. 33 also shows the slab deformations from the mechanical model.

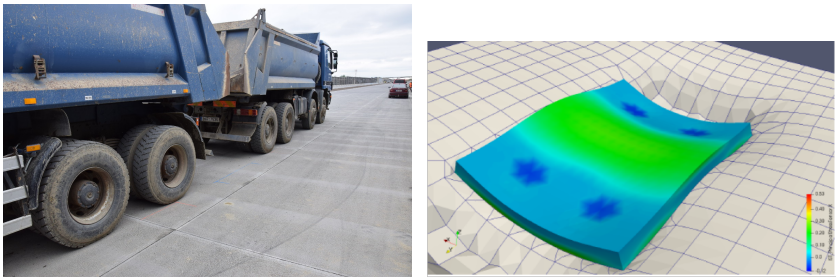

Figure 33: Static load test for a concave deformed shape and displacements.

Fig. 34 shows experimental partial strains, induced due to thermal effects and static loading. While fluctuating temperature induces daily fluctuations ± 10 $\mu\varepsilon$, the truck load induces ± 5 $\mu\varepsilon$ only. The results demonstrate that temperature effects contribute to fatigue as well, which should be reflected better in pavement design codes.

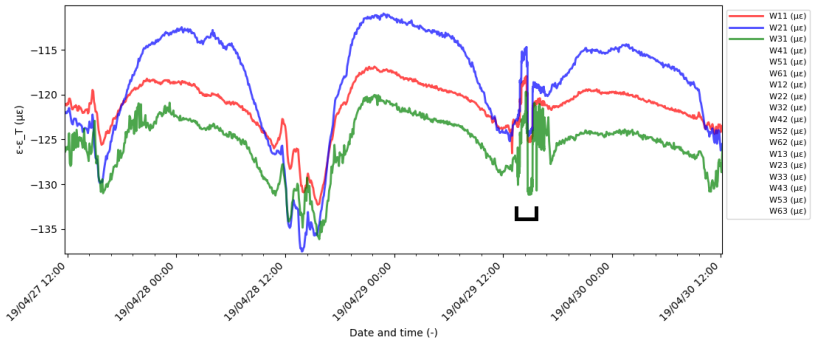

Figure 34: Strains in the top gauges. The brace shows the effect of truck loading.

6 Conclusions and outlook

Slow-hardening binders offer an easy approach to extend the durability and service life of exterior concrete structures. The current explanation is based on invisible microcracks, driven by chemical shrinkage and by a short time for stress relaxation. The fluctuation of temperature, humidity and other strain-inducing mechanisms coalesces the microcracks into visible cracks, increasing permeability and finally disintegrating concrete. The need for fast construction schedules practically eliminated slow-hardening binders from the market and gave rise to crack-prone concretes, exhibiting severe cracking under exterior conditions.

Ring shrinkage tests can reveal binder's resistance to cracking, justified also on 53 year old panels. A longer time for the ring failure means a higher resistance to cracking due to drying. The ring test served for designing crack-resistant slag-blended cement for concrete pavements used on an almost 9 km long, pilot highway section. After three years of slab monitoring, the data show the anticipated behavior both in thermal and mechanical parts. A detailed visual inspection after 3 years showed no visible cracks. This supports the benefits of slow-hardening binders as provided by history lessons. Success in the pilot highway section has triggered revisions for national standards and new specifications for road cements.

7 References

[1] Z. Bažant and M. Jirásek. *Creep and Hygrothermal Effects in Concrete Structures*. Springer, 2018.

[2] Z. Bažant, H. Ohtsubo, and K. Aoh. Stability and post-critical growth of a system of cooling or shrinkage cracks. *Construction and Building Materials*, 15(5):443–456, 1979.

[3] J. Bhatty and P. Tennis. U.S. and Canadian Cement Characteristics: 2004. Technical report, Portland Cement Association, Skokie, Illinois, 2008.

[4] M. Bouasker, P. Mounanga, P. Turcry, A. Loukili, and A. Khelidj. Chemical shrinkage of cement pastes and mortars at very early age: Effect of limestone filler and granular inclusions. *Cement and Concrete Composites*, 30(1):13–22, 2008.

[5] R. W. Burrows. *The visible and invisible cracking of concrete*. ACI International, 1998.

[6] R. Carlson and T. Reading. Model Study of Shrinkage Cracking in Concrete Building Walls. *ACI structural journal*, 85(4):395–404, 1988.

[7] C. Davie and E. Masoero. Modelling damage from the nano-scale up. In *10th International Conference on Mechanics and Physics of Creep, Shrinkage, and Durability of Concrete and Concrete Structures*, 2015.

[8] J. Hlavatý, V. Šmilauer, B. Slánský, and R. Dvořák. Opatření k prodloužení životnosti cementobetonových krytů vozovek - část I. *Silniční obzor*, 80:164–168, 2019.

[9] J. Hlavatý, V. Šmilauer, B. Slánský, and R. Dvořák. Opatření k prodloužení životnosti cementobetonových krytů vozovek - část II. *Silniční obzor*, 80:193–197, 2019.

[10] P. Hlaváček, R. Šulc, V. Šmilauer, C. Rößler, and R. Snop. Ternary binder made of CFBC fly ash, conventional fly ash, and calcium hydroxide: Phase and strength evolution. *Cement and Concrete Composites*, 90:100–107, 2018.

[11] M. Hlobil, V. Šmilauer, and G. Chanvillard. Micromechanical multiscale fracture model for compressive strength of blended cement pastes. *Cement and Concrete Research*, 83:188 – 202, 2016.

[12] K. Hájková, V. Šmilauer, L. Jendele, and J. Červenka. Prediction of reinforcement corrosion due to chloride ingress and its effects on serviceability. *Engineering Structures*, 174:768–777, 2018.

[13] Z. Jiang, Z. Sun, and P. Wang. Autogenous relative humidity change and autogenous shrinkage of high-performance cement pastes. *Cement and Concrete Research*, 35(8):1539 – 1545, 2005.

[14] M. Jirásek and P. Havlásek. Microprestress-solidification theory of concrete creep: Reformulation and improvement. *Cement and Concrete Research*, 60:51–62, 2014.

[15] A. Khan et al. Control of Cracking in Concrete. State of the Art. Technical report, Transportation Research Board, Washington, DC, Oct 2006.

[16] J. Khatib, R. Ramadan, H. Ghanem, and A. Elkordi. Volume stability of cement paste containing limestone fines. *Buildings*, 11(8), 2021.

[17] M. Mac, H. Wong, and N. Buenfeld. 3D characterisation of microcracks in concrete. In M. Dalang-Secrétan, editor, *Nanocem spring meeting in Leimen, Germany*, pages 135–139, 2017.

[18] M. Mac, M. Yio, H. Wong, and N. Buenfeld. Analysis of autogenous shrinkage-induced microcracks in concrete from 3D images. *Cement and Concrete Research*, 144:106416, 2021.

[19] P. Mehta and R. Burrows. Building durable structures in the 21st century. *The Indian concrete journal*, 75(7):437–443, 2001.

[20] P. K. Mehta. Concrete technology at the crossroads–problems and opportunities. In *Concrete Technology Past, Present and Future, SP-144*, pages 1–31. ACI Detroit, 1994.

[21] J. Němeček, V. Králík, V. Šmilauer, L. Polívka, and A. Jäger. Tensile strength of hydrated cement paste phases assessed by micro-bending tests and nanoindentation. *Cement and Concrete Composites*, 73:164–173, 2016.

[22] J. Němeček, V. Šmilauer, J. Němeček, and J. Maňák. Microscale fracture properties of alkali-activated fly ash. In G. Pijaudier-Cabot, P. Grassl, and C. La Borderie, editors, *10th International Conference on Fracture Mechanics of Concrete and Concrete Structures. (FraMCoS-X)*, pages 1 – 8, Bayonne, 2019.

[23] B. Patzák. OOFEM - an object-oriented simulation tool for advanced modeling of materials and structures. *Acta Polytechnica*, 52(6):59–66, 2012.

[24] B. Slánský, V. Šmilauer, J. Hlavatý, and R. Dvořák. New Long-Life Concrete Pavements in the Czech Republic. In *12th International Conference on Concrete Pavements.* International Society for Concrete Pavements, 2021.

[25] V. Šmilauer. *Multiscale hierarchical modeling of hydrating concrete*. Saxe-Coburg Publications, first edition, 2015.

[26] V. Šmilauer, P. Havlásek, T. Gasch, A. Delaplace, D. E.-M. Bouhjiti, F. Benboudjema, M. Briffaut, F. Kanavaris, and M. Azenha. Hygro-mechanical modeling of restrained ring test: COST TU1404 benchmark. *Construction and Building Materials*, 229:116543, 2019.

[27] V. Šmilauer, F. Kolařík, J. Němeček, and J. Maňák. Strength scaling from C-S-H globules to cement paste using multiscale hierarchical modeling. In *Proceedings of the Workshop on Concrete Modelling and Materials Behaviour in honor of Professor Klaas van Breugel*. Rilem Publications S.A.R.L., 2018.

[28] M. Yio, M. Mac, Y. Yeow, H. Wong, and N. Buenfeld. Effect of autogenous shrinkage on microcracking and mass transport properties of concrete containing supplementary cementitious materials. *Cement and Concrete Research*, 150:106611, 2021.

8 Author's main achievements

The author works in the field of micromechanical modeling, cementitious materials, thermo-hygro-mechanical simulations. He has published 63 papers in journals and 126 conference papers. The main achievements include:

Three selected journal articles

- M. Hlobil, V. Šmilauer, G. Chanvillard: Micromechanical multiscale fracture model for compressive strength of blended cement pastes. Cement and Concrete Research. 2016, 83, 188-202. The paper micromechanically proved the empirical gel/space concept introduced by T.C. Powers and quantified the spatial distribution of hydrates on strength. It led to microcrack introduction in order to match experimental data on the cement paste level. It triggered experimental investigation of direct tensile strength assessment on the microscale. *Cited by 61.*
- J. Němeček, V. Králík, V. Šmilauer, L. Polívka, A. Jager: Tensile strength of hydrated cement paste phases assessed by micro-bending tests and nanoindentation. Cement and Concrete Composites. 2016, 73, 164-173. Direct measurement of tensile strength of hydrates. It led to the improvement of multiscale models, introducing microcracks. *Cited by 53.*
- P. Hlaváček, V. Šmilauer, F. Škvára, R. Šulc, L. Kopecký.: Inorganic foams made from alkali-activated fly ash: Mechanical, chemical and physical properties. Journal of the European Ceramic Society. 2015, 35, 703-709. Lab-scale production of foams and their properties under different loading conditions. *Cited by 88.*

Application of new binders

- Slag-blended binder applied on almost 9 km of a road concrete pavement, cast on the D1 highway section Přerov-Lipník nad Bečvou in the period July 23, 2018 - July 2019. The main contractor was Skanska, a.s. Concrete volume reached almost 55,000 m^3. Verified technology of the authors V. Šmilauer, B. Slánský, L. Vysloužil, M. Uhlířová, M. Ohnutek: Use of mixed binders for the construction of cement concrete coverings with extended durability, 2018. The pilot project, including long-term monitoring, successfully verified this solution with crack-resistant cement and is the basis for the revision of the ČSN 73 6123-1 standard Road Construction - Road Concrete Pavements.
- Application of ternary binder, replacing over 1000 tons of clinker in Prague metro D. Primary lining replaces about 45% of CEM I 42.5 R, saving over 700 t of CO_2. Patent P. Růžička, Š. Pešková, V. Šmilauer, R. Sovják, P. Konvalinka: Shotcrete. Czech Republic. Patent CZ 308680. 2021-01-08.
- Design of dam concrete and construction stages in Krounka polder, Kutřín. Concretes with a low amount of binders, utilizing performance-based

design and beyond current codes. Experiments and thermo-mechanical simulations for tender documentation and preliminary desing of water cooling. V. Šmilauer, P. Reiterman, P. Havlásek, P. Huňka, T. Moravec: Krounka, Kutřín, polder construction - verification of basic properties of concrete, Technical Report, 2019.

Selected grants

- Principal investigator of CoreProjekt 10 in the Nanocem consortium (10 industrial partners + up to 32 academic mainly European institutions) "Micromechanical Analysis of Blended Cement-Based Composites" with TU Wien, 2012-2016.
- Principal investigator of the Czech Science Foundation project GAČR 21-03118S "Thermo-hygro-mechanical model of concrete pavements", 2021-2023.

Experimental measurements

- Long-term monitoring of a concrete pavement slab on the D1 highway. 18 vibrating strain gauges, automatic logging and data transfer, installed Aug 8, 2018.
- Long-term monitoring of concrete whitetopping in Rajhrad and Ladná, each 12 strain gauges, 4 displacement gauges, automatic logging and data transfer, installed Sept 22, 2020 and May 4, 2021.
- Long-term monitoring of railway tunnel primary lining - Mezno and Zvěrotice, each 12 strain gauges and temperature gauges, installed May-September 2021.

Software development

- Development and testing of ConTemp+ software for Holcim and LafargeHolcim companies. It is a thermo-mechanical simulator of massive concrete blocks with the possibility of calibration and blind prediction of temperature and crack development. The software is used in 20+ countries around the world, used for Access Tower II, Sri Lanka, the Ecuador turbine foundation, a bridge foundation block in Switzerland, the Bolzum water lock, Germany, etc.
- Development of OOFEM software, an open-source finite-element software in C ++ under the main architect Prof. B. Patzák. Contribution to heat conduction and hydration models, orthotropic material failure model, coupled problems. Application to several engineering applications.

Committee membership

- RILEM international scientific technical committee TC 242-MDC: Multi-decade creep and shrinkage of concrete: material model and structural analysis (2010-2015)
- RILEM TC 254-CMC: Thermal cracking of massive concrete structures (2013-2019)

- COST TU 1404: Towards the next generation of standards for service life of cement-based materials and structures (2014-2018)
- RILEM TC 287-CCS: Early age and long-term crack width analysis in RC structures (2019-)
- Nanocem representative of CTU in Prague 2011-2020, founded 2004, ended 2020.

9 Curriculum vitae

Basic information

Name, titles	Vít Šmilauer, Doc. Ing. Ph.D. DSc.
Date and place of birth	July 10, 1978 in Prague
Position	Associate professor
Employer's address	Czech Technical University in Prague, Department of Mechanics, Thákurova 7, 166 29 Praha 6, Czech Republic
Phone	(+420) 224 354 483
E-mail	vit.smilauer@fsv.cvut.cz
Nationality	Czech

Education and qualification

2018	**DSc.**, Czech Academy of Sciences, Research professor in technical sciences, since Apr 4, 2018.
2003-2006	**Ph.D.**, Czech Technical University in Prague, Faculty of Civil Engineering, Department of Mechanics, Ph.D. thesis: Elastic properties of hydrating cement paste determined from hydration models, defended Jan 12, 2006.
1997-2003	**MSc.**, Czech Technical University in Prague, Faculty of Civil Engineering, Structural and Transportation Engineering. Diploma thesis: Modeling of Hydration of Cement-based Materials: Performance of CEMHYD3D Model, defended June 25, 2003.

Educational exchange

2009-2010	**PostDoc**, Northwestern University, prof. Z.P. Bažant. Multiscale modeling of fracturing and size effect in braided composites for crashworthy lightweight structures. 6 months.
2006-2009	**Visiting scholar**. Northwestern University, USA, visiting scholar, prof. Z.P. Bažant. Multiscale simulation of cement paste creep. 4 months.
2005	**Visiting scholar**. EPFL, LMC, Lausanne, Switzerland, visiting scholar, prof. K. Scrivener. Simulation of hydrating cement paste and elasticity. 2 monhts.
2001	**Junior researcher**, TU Delft, the Netherlands, Faculty of Civil Engineering and Geosciences, undergraduate study in ERASMUS exchange program, prof. K. van Breugel. 4 months.

Professional experience and employment

2009-2022	**Associate professor**, Czech Technical University in Prague, Faculty of Civil Engineering, Department of Mechanics. Teaching of undergraduate and graduate students. Habilitation Dec 18, 2008.
2008-2022	**Reviewer** in Cement and Concrete Research, Cement and Concrete Composites, Ceramics-silikáty, Engineering structures, Fuel, Journal of Materials in Civil Engineering, International Journal of Fracture, Advances in Engineering Software, etc.
2012-2022	**RILEM member** of technical committees TC 242-MDC Multi-decade creep and shrinkage of concrete: material model and structural analysis (2010-2015), TC 254-CMS Thermal cracking of massive concrete structures (2013-2019), TC CCS Cracking of Concrete Structures (2019-).
2014-2018	**COST TU 1404** Management Committee Member: Towards the next generation of standards for service life of cement-based materials and structures. Responsible for material and structural modeling.
2011-2020	**Nanocem representative** of CTU in Prague (industry-academical Pan-European network).
2000-2005	**Structural designer**. Di5 s.r.o. and R-projekt 07. Structural design and analysis of civil engineering structures.

Honors and awards

2017	B. Patzák et al: Software OOFEM, ver. 2.4 obtained excellent grade 1 in national evaluation of selected outputs among institutions (Metodika M17+, Modul 1, grade 1 issued 7× in Engineering and technology).
2017	V. Šmilauer et al: ConTemp - a thermo-mechanical simulator obtained excellent grade 1 in national evaluation of selected outputs among institutions (Metodika M17+, Modul 1, grade 1 issued 7× in Engineering and technology).
2016	J. Němeček, V. Králík, V. Šmilauer, L. Polívka, A. Jäger: Tensile strength of hydrated cement paste phases assessed by microbending tests and nanoindentation. Cement and Concrete Composites, 2016. Selected among the best results from Faculty of Civil Engineering (Metodika M17+, Modul 2).
2016	M. Hlobil, V. Šmilauer, G. Chanvillard: Micromechanical multiscale fracture model for compressive strength of blended cement pastes. Cement and Concrete Research, 2016. Selected among the best results from Faculty of Civil Engineering (Metodika M17+, Modul 2).
2014	F. Škvára, L. Kopecký, V. Šmilauer, Z. Bittnar: Material and structural characterization of alkali activated low-calcium brown coal fly ash. Journal of Hazardous Materials, 2009. Selected as the second best result from the Faculty of Civil Engineering during R&D Council evaluation for Pillar II – excellence science.
2011	"Excellent concrete structure" awarded by the Czech Concrete Society – Oparno bridge built by Metrostav. Design of water cooling pipes in the arch for heat mitigation.
2006	Rector's award for an excellent Ph.D. thesis.
2003	Prize of Josef Hlávka.
2002	The first place in the competition "Prize of the academician prof. Bažant" at CTU in Prague.

Teaching activities

2003-2022	Undergraduate students: Theory of elasticity, Structural mechanics, Finite element method, Structural dynamics. Graduate students: Micromechanics of cementitious composites.

Selected research projects and contracts

2020-2024	Co-executor of EU Horizon 2020 EURATOM No. 900012 – ACES – NFRP-2019-2020 "Towards improved assessment of safety performance for long-term operation of nuclear civil engineering structures"
2021-2023	Principal investigator of GAČR 21-03118S "Thermo-hygro-mechanical model of concrete pavements"
2018-2019	Principal investigator of the contract with Povodí Labe, s.p. "Krounka, Kutřín, construction of the polder - verification of basic properties of concrete"
2018-2022	Principal investigator of the contract with Skanska, a.s. Monitoring of cement concrete cover D1 Přerov-Lipník nad Bečvou. Monitoring of whitetoppping of D52 Rajhrad. Contract with Metrostav, a.s .: Monitoring of whitetopping of D2 Ladná
2018-2020	Project co-executor in the project TAČR TH03020404 "Extending service life of concrete road pavements using mineral admixtures and blended cements" from the Technology Agency of the Czech Republic.
2017-2021	Participation in the project EU Horizon 2020 Project. Contract No. 721105 "Multi-scale Composite Material Selection Platform with a Seamless Integration of Materials Models and Multidisciplinary Design Framework"
2013-2019	Participation in the project TAČR TE01020168 "Centre for Effective and Sustainable Transport Infrastructure (CESTI)"
2015-2017	Project co-executor in the project TAČR TA04031458 "Software for prediction and modelling of durability and safety of transportation structures" from the Technology Agency of the Czech Republic.

2014-2016	Participation in the FP7 project “Multiscale Modelling Platform: Smart Design of nano-enabled products in green technologies”, THEME NMP.2013.1.4-1 Development of an integrated multi-scale modelling environment for nanomaterials and systems by design. No. 604279.
2012-2016	Project executor in Nanocem’s industrially funded core project CP10 “Micromechanical analysis of blended cement-based composites”
2012-2014	Project executor in the research project "Aluminosilicate polymer foams" from the Czech Science Foundation, P104/12/0102.
2005-2011	Participation in the MŠMT grant “Evolution of computer algorithms and simulation and their application in civil engineering”, MSM 684077000.

Software development

2008-2022	Team member of OOFEM, package for object-oriented finite element method – www.oofem.org, written in C++, the main architect Prof. B. Patzák.
2012-2017	Main coordinator of ConTemp+ software development, multiscale thermo-mechanical tool for hydrating concrete blocks, C++, supported by LafargeHolcim company. Software used in 20+ countries around the world for predicting concrete temperature and cracking during hydration.

Selected peer-reviewed publications

Peer-reviewed articles in Web of Science 51. WoS times cited 1101, without self-citation 1058, h-index 17.

1. C. Pohl, V. Šmilauer, J. Unger: A Three-Phase Transport Model for High-Temperature Concrete Simulations Validated with X-ray CT Data. Materials. 2021, 14, 1-21.
2. P. Havlásek, V. Šmilauer, L. Dohnalová, R. Sovják: Shrinkage-induced deformations and creep of structural concrete: 1-year measurements and numerical prediction, Cement and Concrete Research, 2021.
3. S. Šulc, V. Šmilauer, F. Wald: Thermal Model for Timber Fire Exposure with Moving Boundary. Materials. 2021, 14(3), 1-10.

4. V. Šmilauer, P. Havlásek, T. Gasch, A. Delaplace, D. E.-M. Bouhjiti, F. Benboudjema, M. Briffautf, F. Kanavaris, M. Azenha: Hygro-mechanical modeling of restrained ring test: COST TU1404 benchmark. Construction and Building Materials, 2019.
5. S. Šulc, V. Šmilauer, B. Patzák, K. Cábová, F. Wald:: Linked simulation for fire-exposed elements using CFD and thermo-mechanical models. Advances in Engineering Software, 2019, 131, 12-22.
6. K. Hájková, V. Šmilauer, L. Jendele, J. Červenka: Prediction of reinforcement corrosion due to chloride ingress and its effects on serviceability. Engineering Structures, 2018, 174, 768-777.
7. A. Jedrzejewska, F. Benboudjema, L. Lacarrière, M. Azenha, D. Schlicke, S. Dal Pont, A. Delaplace, J. Granja, K. Hájková, P. J. Heinrich, G. Sciumè, E. Strieder, E. Stierschneider, V. Šmilauer, V. Troyan: COST TU1404 Benchmark on macroscopic modelling of concrete and concrete structures at early age: proof-of-concept stage. Construction and Building Materials. 2018, 174, 173-189.
8. P. Hlaváček, R. Šulc, V. Šmilauer, C. Roessler, R. Snop: Ternary binder made of CFBC fly ash, conventional fly ash, and calcium hydroxide: Phase and strength evolution. Cement and Concrete Composites. 2018, 90, 100-107.
9. U. Haider, Z. Bittnar, L. Kopecký, V. Šmilauer, J. Pokorný, M. Záleská, Z. Prošek, V. Hrbek: Determining the role of individual fly ash particles in influencing the variation in the overall physical, morphological, and chemical properties of fly ash. Acta Polytechnica. 2016, 56(4), 265-282.
10. J. Němeček, V. Králík, V. Šmilauer, L. Polívka, A. Jäger: Tensile strength of hydrated cement paste phases assessed by microbending tests and nanoindentation. Cement and Concrete Composites. 2016, vol. 73, 164-173.
11. M. Hlobil, V. Šmilauer, G. Chanvillard: Micromechanical multiscale fracture model for compressive strength of blended cement pastes, Cement and Concrete Research, 2016, vol. 83, 188-202.
12. P. Hlaváček, V. Šmilauer, F. Škvára, R. Šulc, L. Kopecký.: Inorganic foams made from alkali-activated fly ash: Mechanical, chemical and physical properties. Journal of the European Ceramic Society. 2015, vol. 35, no. 2, 703-709.
13. W. da Silva, V. Šmilauer, P. Štemberk: Upscaling semi-adiabatic measurements for simulating temperature evolution of mass concrete structures. Materials and Structures. 2015, vol. 48, no. 4, 1031-1041.
14. F. Škvára, V. Šmilauer, P. Hlaváček, L. Kopecký, Z. Cílová: A weak alkali bond in (N, K)-A-S-H gels: evidence from leaching and modeling. Ceramics - Silikáty. 2012, vol. 56, no. 4, 374-382.
15. J. Vorel, V. Šmilauer, Z. Bittnar: Multiscale Simulations of Concrete

Mechanical Tests. Journal of Computational and Applied Mathematics. 2012, vol. 236, no. 18, 4882-4892.
16. J. Němeček, V. Šmilauer, L. Kopecký.: Nanoindentation characteristics of alkali-activated aluminosilicate materials. Cement and Concrete Composites. 2011, vol. 33, no. 2, 163-170.
17. V. Šmilauer, Z.P. Bažant: Identification of viscoelastic C-S-H behavior in mature cement paste by FFT-based homogenization method. Cement and Concrete Research. 2010, vol. 40, no. 2, 197-207.
18. V. Šmilauer, T. Krejčí: Multiscale Model for Temperature Distribution in Hydrating Concrete. International Journal for Multiscale Computational Engineering. 2009, vol. 7, no. 2, 135-151.
19. F. Škvára, L. Kopecký, V. Šmilauer, Z. Bittnar: Material and structural characterization of alkali activated low-calcium brown coal fly ash. Journal of Hazardous Materials. 2009, vol. 168, no. 2-3, 711-720.
20. V. Šmilauer, Z. Bittnar: Microstructure-based Micromechanical Prediction of Elastic Properties in Hydrating Cement Paste. Cement and Concrete Research. 2006, vol. 36, no. 9, 1708-1718.

Books

1. V. Šmilauer: Multiscale Hierarchical Modeling of Hydrating Conctrete. First edition. Stirlingshire: Saxe-Coburg Publications, 2015. 164 pages, ISBN 978-1-874672-51-7.

České vysoké učení technické v Praze
Název: Crack-resistant binders for durable concrete structures / Trhlinkovzdorná pojiva pro trvanlivé betonové konstrukce
Autor: doc. Ing. Vít Šmilauer, Ph.D., DSc.
Tisk: Ottova tiskárna, s.r.o., U Stavoservisu 527/1, 108 00 Praha 10
1. vydání

ISBN 978-80-01-06924-0